Gating Currents from K_v7 Channels Carrying Neuronal Hyperexcitability Mutations in the Voltage-Sensing Domain

Francesco Miceli,[†‡§] Ernesto Vargas,[§] Francisco Bezanilla,[§*] and Maurizio Taglialatela[†¶*]

[†]Section of Pharmacology, Department of Neuroscience, University of Naples Federico II, Naples, Italy; [‡]Division of Neurology, IRCCS Bambino Gesù Children's Hospital, Rome, Italy; [§]Department of Biochemistry and Molecular Biology, The University of Chicago, Chicago, Illinois; and [¶]Department of Health Science, University of Molise, Campobasso, Italy

ABSTRACT Changes in voltage-dependent gating represent a common pathogenetic mechanism for genetically inherited channelopathies, such as benign familial neonatal seizures or peripheral nerve hyperexcitability caused by mutations in neuronal $K_v7.2$ channels. Mutation-induced changes in channel voltage dependence are most often inferred from macroscopic current measurements, a technique unable to provide a detailed assessment of the structural rearrangements underlying channel gating behavior; by contrast, gating currents directly measure voltage-sensor displacement during voltage-dependent gating. In this work, we describe macroscopic and gating current measurements, together with molecular modeling and molecular-dynamics simulations, from channels carrying mutations responsible for benign familial neonatal seizures and/or peripheral nerve hyperexcitability; $K_v7.4$ channels, highly related to $K_v7.2$ channels both functionally and structurally, were used for these experiments. The data obtained showed that mutations affecting charged residues located in the more distal portion of S_4 decrease the stability of the open state and the active voltage-sensing domain configuration but do not directly participate in voltage sensing, whereas mutations affecting a residue (R4) located more proximally in S_4 caused activation of gating-pore currents at depolarized potentials. These results reveal that distinct molecular mechanisms underlie the altered gating behavior of channels carrying disease-causing mutations at different voltage-sensing domain locations, thereby expanding our current view of the pathogenesis of neuronal hyperexcitability diseases.

INTRODUCTION

Translocation of charged particles (termed gating charges) within the membrane electric field is responsible for activation of the conductance in voltage-gated ion channels (VGICs). Positively charged lysines (K) or arginines (R) within the fourth transmembrane segment (S_4) are the main gating charges in voltage-gated *Shaker* K^+ channels (1–4) and possibly in most Na^+, Ca^{2+}, and K^+ channels (5,6). In addition to S_4 charged residues, negatively charged residues in S_2 (2) and hydrophobic residues in S_1, S_2, and S_3, defining the extent of the electric field where the charges translocate (7–10), have been shown to contribute to the gating process; thus, the region comprising S_1 through S_4 represents the voltage-sensing domain (VSD) of VGICs.

Changes in channel gating represent a common pathogenetic mechanism for genetically inherited channelopathies affecting heart rhythm, skeletal muscle contraction, or neuronal excitability. In particular, gating alterations play a major role in the pathogenesis of benign familial neonatal seizures (BFNS) (11–14), a rare autosomal-dominant idiopathic epilepsy of the newborn caused by mutations in the genes encoding for $K_v7.2$ (15,16) or, more rarely, $K_v7.3$ (17). $K_v7.2$ and $K_v7.3$ subunits underlie the M-current (I_{KM}), a slowly activating and deactivating K^+ current that regulates neuronal excitability in the subthreshold range for action-potential generation. I_{KM}-forming $K_v7.2$ and $K_v7.3$ subunits are widely distributed in hippocampal, neocortical, and cerebellar neurons, at key sites for network oscillations and synchronization control (18); in these neurons, in addition to somatodendritic compartments, $K_v7.2$ and $K_v7.3$ subunits appear to be mainly localized at the axon initial segment (19), at Ranvier nodes (20), and at synaptic terminals (21). Among the other members of the K_v7 gene family, $K_v7.1$ is mainly expressed in the heart muscle and $K_v7.4$ in cochlear and vestibular organs of the inner ear, as well as in central auditory pathways, visceral and vascular smooth muscle, and skeletal muscle, whereas $K_v7.5$, in addition to neurons, has been also detected in human adult skeletal muscle and in vascular smooth muscle cells (22).

In $K_v7.2$, most BFNS-causing mutations are localized either in the large intracellular C-terminal domain, a critical region for subunit assembly and channel regulation, or in the VSD (14). A mild decrease of I_{KM} appears sufficient to cause BFNS, and haploinsufficiency seems the primary pathogenetic mechanism for both familial and sporadic forms of the disease. Although some mutations affect intracellular protein trafficking and polarized targeting (23,24), others reduce channel sensitivity to voltage and stabilize the closed-state conformation (11–13). However, genotype-phenotype correlations in BFNS-affected individuals are weak, and the intimate causes for the complex constellation of neurological signs and symptoms in $K_v7.2$-mutation carriers are only poorly understood.

Submitted December 19, 2011, and accepted for publication February 7, 2012.

*Correspondence: m.taglialatela@unimol.it or fbezanilla@uchicago.edu

Editor: Chris Lingle.

0006-3495/12/03/1372/11 $2.00

doi: 10.1016/j.bpj.2012.02.004

Functional consequences of disease-causing mutations in K_v7 channels have been mostly studied by means of macroscopic current measurements, a technique unable to provide a detailed assessment of the subtle functional changes in voltage sensing and of the potential structural consequences underlying altered gating behavior; instead, analysis of the gating currents can provide a direct measure of gating-charge translocation during VSD displacement upon channel gating. In this work, we performed macroscopic and gating-current measurements in K_v7 channels carrying mutations responsible for BFNS and/or peripheral nerve hyperexcitability (PNH) (11,25–27). Since gating currents from $K_v7.2$ channels could not be resolved, the experiments were carried out in the functionally-and structurally-related $K_v7.4$ channels.

The data obtained show that mutations affecting charged residues located in the more distal portion of S_4 decrease the stability of the open state and of the active VSD configuration but do not directly participate in voltage sensing, whereas mutations affecting a residue (R4) located more proximally in S_4 caused gating-pore currents activating at depolarized potentials. These results reveal that distinct molecular mechanisms underlie the altered gating behavior of channels carrying mutations at different VSD locations, thereby expanding our current view of the pathogenesis of neuronal hyperexcitability diseases.

MATERIALS AND METHODS

Isolation of *Xenopus* oocytes

The dissociation, maintenance, and microinjection of *Xenopus* oocytes followed standard procedures (28).

cDNA transcription and oocyte injection

K_v7 cDNAs were cloned in pTLN vectors. Mutations were introduced by PCR using degenerated primers (QuickChange, Stratagene, Milan, Italy) and verified by sequencing. Plasmid linearization and in vitro transcription followed standard procedures (28).

Vaseline-gap cut-open voltage-clamp electrophysiology

Ionic and gating currents from *Xenopus* oocytes were measured at 28°C, as previously described (29,30), using a Peltier device with a negative-feedback thermistor as a temperature sensor. The composition of the external and internal solutions for ionic current recordings were (in mM) 101 *N*-methy-D-glucamine (NMG), 12 KOH, 4 $Ca(OH)_2$, and 20 Hepes, pH 7.4 with methane sulfonic acid (MES acid), and 120 KOH, 2 EGTA, and 20 Hepes, pH 7.4 with MES acid, respectively. For gating-current recordings, the external and internal solutions contained (in mM) 100 tetraethylammonium-hydroxide (TEA-OH), 2 $Ca(OH)_2$, 2 Ba^{2+}, and 20 Hepes, pH 7.4 with MES acid, and 115 TEA-OH, 2 EGTA, and 20 Hepes, pH 7.4 with MES acid, respectively. Oocytes were permeabilized by adding 0.3% saponin to the lower chamber for ~1 min. Microelectrodes were pulled from borosilicate glass capillary tubes to obtain a resistance of 0.1–0.5 MΩ when filled with 3 M CsMES + 20 mM CsCl. Ionic currents were activated by depolarizing pulses of 1.5-s duration from −100 to +40 mV from a holding potential of −90 mV, followed by an isopotential pulse at −90 mV of 800–1500 ms. Capacity currents were compensated by analog circuitry and subtracted off-line. The data acquisition system was built in-house based on an Innovative Integration SB6711 with A4D4 boards running with in-house-written software. Ionic-current data were filtered at 1–2 kHz and sampled at 2–4 kHz. For gating-current recordings, oocytes were maintained at 0 mV for 30 min to deplete intracellular K^+; after this period, the cells were exposed to the TEA-based solutions (± external Ba^{2+}), and the following protocol was applied: from a holding potential of −90 mV, a 20-ms pulse to −100 mV was followed by voltage steps from −80 mV to +80 mV of 70-ms duration before a final 70-ms step to −100 mV was applied. Data were filtered at 5 kHz and sampled at 50 kHz. Capacity currents were compensated by analog circuitry and subtracted on-line using a $p/-8$ protocol from a subtracting holding potential of −100 mV.

Data analysis and statistics

To minimize the effect of extracellular K^+ accumulation, conductance (G) values were calculated as previously described (28). G values were expressed as a function of membrane potential (G/V curves), and the obtained data were fit to a Boltzmann distribution of the following form: $y = \max/[1 + \exp(zF(V_{1/2} - V)/RT)]$, where V is the test potential, $V_{1/2}$ is the half-activation potential, z is the effective valence, and F, R, and T have their usual thermodynamic meanings. Activation and deactivation kinetics were analyzed by fitting the current traces with a single-or a double-exponential equation (12). For the traces fit with a double exponential (calculated with the equation $\tau = (\tau_F A_f + \tau_s A_s)/(A_f + A_s)$, a single time constant was thus obtained that represented the weighted average of the slow and fast components.

In gating-current recordings, the gating charge (Q) was calculated as the time integral of the gating currents (Ig) at each potential after leak subtraction. Q was plotted as a function of membrane potential (Q/V curves), and the data were then fit to the previously described form of the Boltzmann equation. Q_{ON} and Q_{OFF} kinetics were obtained by fitting the integrated Ig_{ON} and Ig_{OFF} traces, respectively, with a single-or a double-exponential equation.

Data are expressed as the mean ± SE of the given number of experiments (n). Data sets were compared using matched Student's t-tests or, if necessary, one-way ANOVA, followed by the Newman Keul's test. In the figures, values statistically different from those of the respective controls ($p < 0.05$) are indicated by asterisks (see Figs. 2 and 3).

Computational modeling

Homology models of the VSDs of $K_v7.4$ and $K_v7.4$ R4Q channels were generated using the software package MODELER v9.8. Structural coordinates from $K_v1.2$ were used as a template. CHARMM-GUI provided scripts for building a membrane system with explicit solvent. The full system was energy minimized and then equilibrated for 0.23 ns. Upon equilibration, a free MD simulation was performed over 10 ns to observe the dynamics of our model.

RESULTS

General features of the gating currents from $K_v7.4$ channels

K_v7 subunits display a core domain formed by six transmembrane segments (S_1–S_6), and cytoplasmic N- and C-termini (Fig. 1 *A*). S_4 primary sequence alignment among several K_v channels, including all K_v7 members, shows

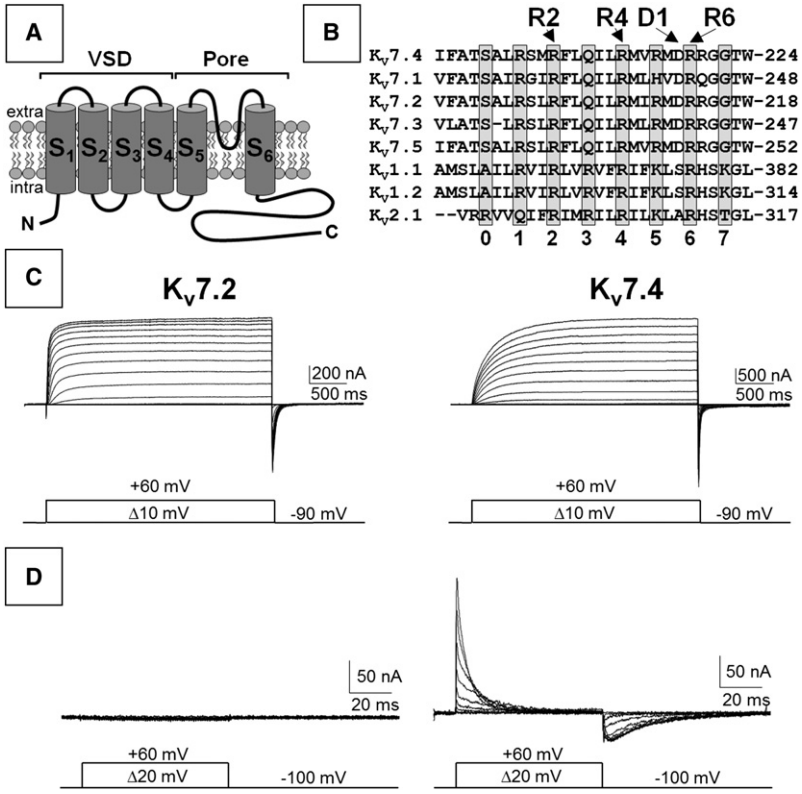

FIGURE 1 Ionic currents from $K_v7.2$ and $K_v7.4$ channels and gating currents from $K_v7.4$ channels. (*A*) Schematic representation of a K_v subunit. (*B*) Sequence alignment of the S_4 segments of the indicated K_v subunits (http://www.ebi.ac.uk/Tools/emboss/align/); residues mutated in this study are indicated at the top. Gray boxes indicate positively charged residues (numbered 0–7). (*C*) Representative macroscopic currents recorded from $K_v7.2$ (*left*) or $K_v7.4$ (*right*) channels expressed in *Xenopus* oocytes, in response to the indicated voltage protocols. (*D*) Representative currents recorded from $K_v7.2$- (*left*) or $K_v7.4$-expressing (*right*) oocytes after blockade of the ionic currents, in response to the indicated voltage protocols.

a variable number of positive charges (numbered 0–7) (Fig. 1 *B*). Characteristic in all subunits of the K_v7 subfamily is the presence of an uncharged Q residue at the position corresponding to R3 and a negatively charged D residue (D1) immediately before the R6 charge. Within the sequence shown, $K_v7.2$ and $K_v7.4$ subunits differ at only three positions, all occupied by hydrophobic residues; in the entire VSD, $K_v7.2$ and $K_v7.4$ primary sequences are ~90% similar. This high degree of primary sequence homology between $K_v7.2$ and $K_v7.4$ must be highlighted as very relevant for the study of this sensor.

In *Xenopus* oocytes at 28°C, both homomeric $K_v7.2$ and $K_v7.4$ channels give rise to voltage-dependent K^+ currents that have a threshold of activation around −50 mV and display slow activation and deactivation kinetics (Fig. 1 *C*). After ionic current blockade with intracellular and extracellular perfusion using K^+-free and tetraethylammonium (TEA)-based solutions in the presence of 2 mM extracellular Ba^{2+}, fast and transient time- and voltage-dependent currents corresponding to the ON and OFF gating currents (Ig_{ON} and Ig_{OFF}, respectively) were recorded from $K_v7.4$-expressing cells (Fig. 1 *D*). Ig_{ON} showed a quasi-instantaneous activation followed by a decay that was faster during stronger depolarization; no residual current was detected at the end of a 70-ms depolarizing pulse to >0 mV. On the other hand, Ig_{OFF} showed a rising phase followed by a slower time-dependent decay. Notably, 2 mM Ba^{2+} did not influence Ig_{ON} and Ig_{OFF} properties of $K_v7.4$ channels; in fact, $V_{1/2}$ values were −26.7 ± 0.6 mV and −30.7 ± 0.9 mV, and z values were 1.93 ± 0.14 and 1.8 ± 0.14 for Q_{ON}/V with or without, respectively, extracellular Ba^{2+} ($n = 4$–10).

By contrast, no gating currents could be detected in oocytes expressing homomeric $K_v7.2$ channels (Fig. 1 *D*) or heteromeric $K_v7.2/K_v7.3$ channels (28), possibly because of a lower density of functional channels in the plasma membrane and a reduced temperature sensitivity of the activation kinetics of $K_v7.2$ channels when compared to $K_v7.4$ channels (28,31). Among K_v7 channels, $K_v7.4$ channels display the lowest single-channel conductance and opening probability (32); thus, the fact that the maximal density of macroscopic currents in $K_v7.4$- and $K_v7.2/K_v7.3$-expressing oocytes was similar suggests that the number of functional $K_v7.4$ channels was the highest among K_v7 channel subtypes. Moreover, it has been observed that most K_v7 channels appear to be present in the plasma membrane in a functionally silent (nonconductive) state, further complicating the interpretation of biochemical data (31,33).

Nonetheless, the fact that gating currents could not be recorded for $K_v7.2$, whereas these could be resolved adequately in $K_v7.4$-expressing oocytes, combined with the described sequence similarity in VSD primary sequence (particularly within S_4) between $K_v7.2$ and $K_v7.4$ subunits, prompted us to investigate to what extent $K_v7.4$ channel gating resembled that of $K_v7.2$ channels, and, in particular, to verify whether mutations in the VSD could prompt similar gating changes when incorporated into $K_v7.2$ or

$K_v7.4$ channels. To this end, we neutralized the charge at the R2 position (R2Q mutation). In $K_v7.2$, such neutralization generated channels retaining all of the pore properties (single-channel conductance, opening probability, K^+ selectivity, and sensitivity to blockade by external TEA) of wild-type channels, but it dramatically modified channel gating properties: $K_v7.2$ R2Q channels carried time-and voltage-independent currents (34) (Fig. 2 *A*), a result suggesting that the R2Q mutation locked the VSD in the active state. Gating changes identical to those described for $K_v7.2$ were also observed when the R2Q mutation was incorporated into $K_v7.4$ channels (Fig. 2 *A*). Similar functional consequences have been also observed when the corresponding mutation was introduced into $K_v7.1$ channels (35), allowing us to further generalize the fundamental role of the R2 charge in VSD resting-state stabilization in channels of the K_v7 subfamily. Moreover, although $K_v7.4$ and $K_v7.4$ R2Q channels exhibited similar macroscopic current amplitudes (Fig. 2 *B*), Ig_{ON} and Ig_{OFF} could not be recorded from $K_v7.4$ R2Q-expressing cells (Fig. 2 *C*), confirming that charge neutralization at R2 effectively impeded VSD return to the resting state.

Altogether, these results suggest the existence of marked analogies between homomeric $K_v7.2$ and $K_v7.4$ channels in the VSD structural transitions that occur during voltage sensing; therefore, $K_v7.4$ channels represent surrogates for $K_v7.2$ that are suitable for investigating the functional effects of disease-causing mutations on both ionic and gating currents.

Molecular mechanisms of channel dysfunction by $K_v7.4$ mutations in the C-terminal region of S_4

Based on the previous conclusions, we introduced at the corresponding positions of $K_v7.4$ some S_4 mutations that cause BFNS and/or PNH when present in $K_v7.2$. We initially focused on two mutations affecting residues located in the S_4 C-terminal region: R6W, a heterozygous germ-line mutation responsible for BFNS in two children from the same family (26), and D1G, found in a sporadic case of BFNS (27), which affected the negatively charged aspartate immediately preceding R6. Moreover, to investigate the differential role of charge and bulkiness at R6, the R6Q mutation was also studied.

At the macroscopic current level, all three mutations (R6W, R6Q, and D1G) caused rightward shifts of ~30 mV in the $V_{1/2}$ of the *G/V* curves of Kv7.4 channels (Fig. 3, *A* and *B*, and Table 1). Activation and deactivation kinetics for R6W, R6Q, and D1G channels were significantly faster than for wild-type channels (Fig. 2, *D* and *E*, and Table 1). Similar functional changes were described when the corresponding mutations were introduced in $K_v7.2$ channels. In fact, the macroscopic currents carried by D1G- (27), R6Q- (34), and R6W-carrying $K_v7.2$ channels (36) displayed a reduced sensitivity to voltage in their steady-state *G/V* curves, together with an acceleration of both activation and deactivation kinetics.

Gating-current analysis in $K_v7.4$ channels carrying the R6W, R6Q, or D1G mutations showed a right shift by 13, 8, and 6 mV, respectively, in the $V_{1/2}$ of the Q_{ON}/V relationships (Fig. 3, *A* and *C*, and Table 1). Qualitatively similar results were observed in the $V_{1/2}$ of the Q_{OFF}/V (Table 1). All three mutations reduced the slopes of the Q_{ON}/V and Q_{OFF}/V relationships, with the R6W causing the largest degree of change (Table 1). Ig_{ON} decay kinetics in R6Q and D1G channels were not affected; the time constants were 5.9 ± 0.5 ms, 5.4 ± 0.4 ms, and 5.7 ± 0.6 ms for wild-type, R6Q, and D1G channels, respectively. Only for R6W channels were Ig_{ON} decay kinetics slightly slower (10.7 ± 0.4 ms; $p < 0.05$ versus wild-type channels). As

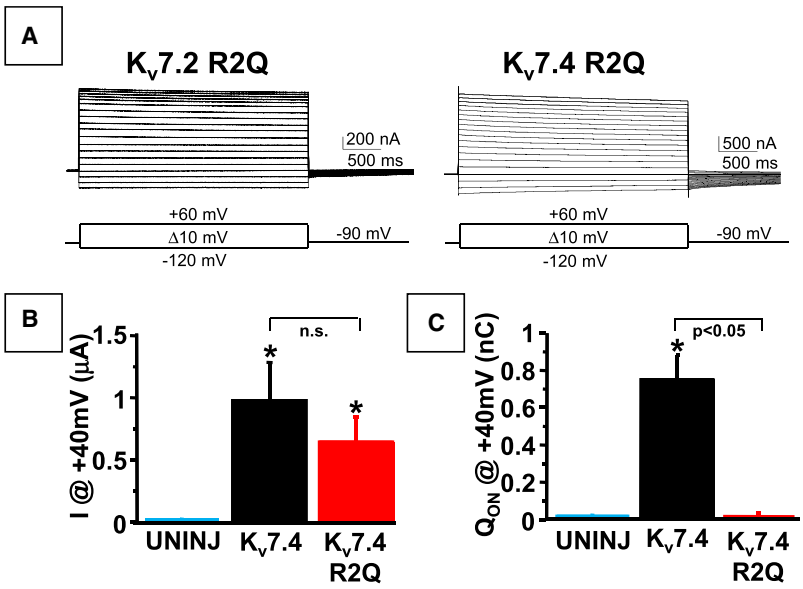

FIGURE 2 Functional effects of the R2Q mutation in S_4 in $K_v7.2$ and $K_v7.4$ channels. (*A*) Representative ionic current traces recorded from oocytes expressing $K_v7.2$ R2Q (*left*) and $K_v7.4$ R2Q (*right*) channels, in response to the indicated voltage protocols. (*B*) Averaged values of peak macroscopic current amplitudes at +40 mV (n = 6–13). (*C*) Averaged values of peak Q_{ON} at +40 mV (n = 6–13).

TABLE 1 Gating properties of S_4 $K_v7.4$ mutants

		G				Q_{ON}			Q_{OFF}		
	n	$V_{1/2}$ (mV)	z (e^-)	Activation τ (ms)	Deactivation τ (ms)	n	$V_{1/2}$ (mV)	z (e^-)	Q at +40 mV (nC)	$V_{1/2}$ (mV)	z (e^-)	Q at +40 mV (nC)
Wt	10	−18.4 ± 0.7	2.04 ± 0.11	212 ± 37* (0 mV)	130 ± 11 (−20 mV) 21.7 ± 2 (−100 mV)	10	−24.1 ± 0.5	1.93 ± 0.14	1.2 ± 0.2	−28.4 ± 0.5	1.9 ± 0.13	1 ± 0.3
R4Q	4	+16 ± 1*	1.43 ± 0.48*	576 ± 31* (0 mV)	258 ± 31* (−20 mV)	10	nd	nd	nd	+12 ± 1*	1.51 ± 0.16*	0.62 ± 0.1*
R4W	4	+32.3 ± 0.7*	1.81 ± 0.48	6590† (0 mV)	3866† (−20 mV)	5	nd	nd	nd	nd	nd	0.26 ± 0.01*
D1G	4	+9.1 ± 0.5*	2.18 ± 0.07	37 ± 11* (0 mV)	27 ± 5* (−20 mV) 6.8 ± 1.4* (−100 mV)	4	−17.9 ± 2.3*	1.38 ± 0.22*	0.8 ± 0.2	−13.2 ± 1.7*	1.38 ± 0.12*	1 ± 0.3
R6Q	6	+11.2 ± 0.7*	2.01 ± 0.16	142 ± 12* (0 mV)	41 ± 6* (−20 mV) 14.8 ± 3.6* (−100 mV)	7	−15.9 ± 0.9*	1.44 ± 0.04*	0.84 ± 0.2	−15.9 ± 0.5*	1.39 ± 0.06*	0.93 ± 0.2
R6W	6	+11.1 ± 1.4*	1.47 ± 0.16*	134 ± 27* (0 mV)	54 ± 12* (−20 mV) 10.9 ± 3.3* (−100 mV)	5	−11 ± 1.5*	1.03 ± 0.07*	1.3 ± 0.3	−14.5 ± 1.1*	1.09 ± 0.06*	1.2. ± 0.3

nd, not determined.
*Significantly different ($p < 0.05$) from the corresponding value in wild-type Kv7.4 channels.
†Due to the extremely slow activation and deactivation kinetics for the R4W channels, the data shown are from a single cell in which longer (8-s) depolarizing and repolarizing pulses were utilized.

a result, the large difference between the slow macroscopic current activation kinetics and the fast Ig_{ON} decay, characteristic of wild-type channels, was reduced in all three mutants (Fig. 3 *D*). By contrast, Ig_{OFF} rising phase was largely abolished in R6W, R6Q, and D1G mutant $K_v7.4$ channels (Fig. 3 *A*); moreover, when compared to wild-type channels, Ig_{OFF} decay kinetics were also faster for all three mutant channels (Fig. 3 *E*). In all channels examined, Ig_{OFF} decay kinetics could be superimposed on those of ionic current deactivation (Fig. 3 *E*).

Molecular mechanisms of channel dysfunction by $K_v7.4$ mutations in the central region of S_4

In $K_v7.2$ channels, mutations affecting the R4 residue have been associated with hyperexcitability disorders. For example, the R4W mutation was observed in patients affected with BFNS and PNH (11), and the R4Q mutation was noted in a family affected by PNH in the reported absence of BFNS (25).

Ionic currents from R4Q or R4W Kv7.4 channels displayed a positive shift in their $V_{1/2}$, which was larger in R4W (~50 mV) than in R4Q (~30 mV) channels (Fig. 4, *A* and *B*, and Table 1). A decrease in activation and deactivation rates was also observed, which appeared more dramatic for R4W-than for R4Q-carrying channels; similar changes in the kinetics and steady-state properties of the macroscopic currents were observed when the corresponding mutations were incorporated in Kv7.2 channels (11,25). After ionic current suppression in both R4Q and R4W channels, depolarizing pulses to >0 mV revealed the appearance of nonlinear currents with complex kinetics; the fast transient Ig_{ON} was followed by a persistent noninactivating current whose magnitude increased upon further membrane depolarization (Fig. 4, *C* and *D*), thus preventing a detailed analysis of Ig_{ON} kinetics and Q_{ON}/V properties. At +80 mV, the magnitude of this current was four and two times larger in R4Q and R4W channels, respectively, when compared to wild-type channels. Upon membrane repolarization to −100 mV, in both mutant channels, an instantaneously rising Ig_{OFF} was recorded, which decayed with a double-exponential time constant, having a fast (~0.5-ms) followed by a slower (~12-ms) component (data not shown); the Q_{OFF}/V curve was right-shifted by ~40 mV, also showing a slightly decreased steepness (Table 1).

The magnitude of the depolarization-induced persistent outward current was directly proportional to the number of channels in the oocyte membrane (estimated by Q_{OFF} measurements) (Fig. 4 *E*), suggesting that the current flowed through these same channels. No apparent changes in the reversal potential of the persistent outward current from R4Q mutant channels were observed when Na^+, K^+, or Li^+ were present in the extracellular solution, suggesting poor current selectivity for monovalent cations (data not shown); the fact that both internal and external solutions

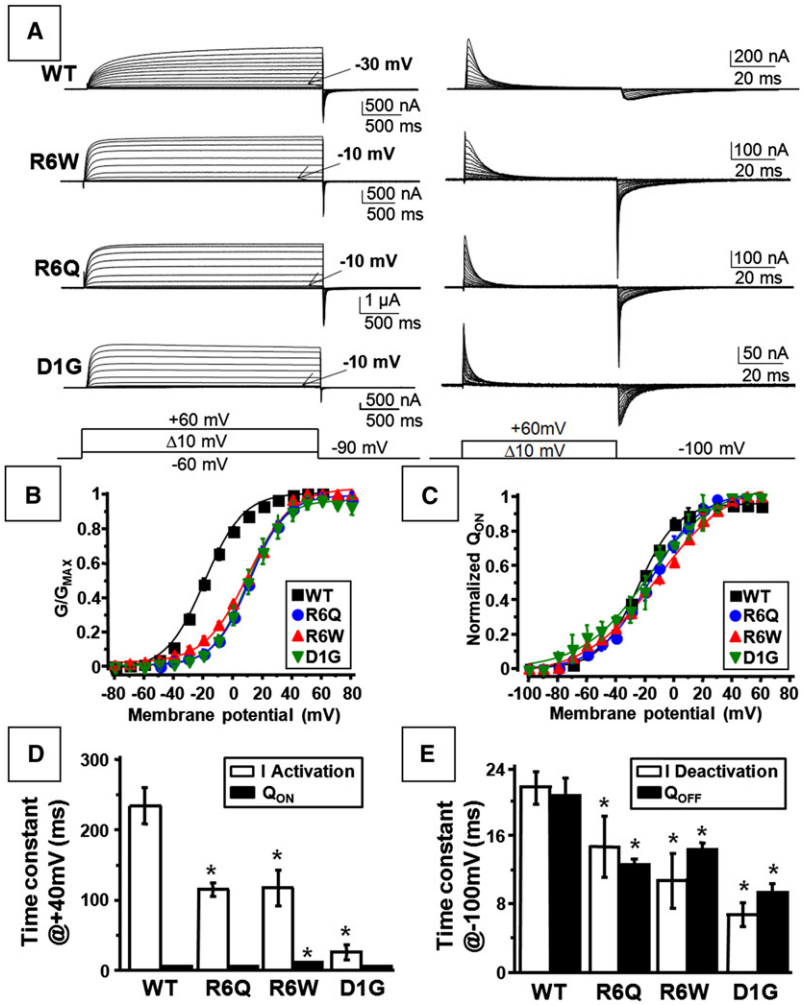

FIGURE 3 Ionic and gating currents from $K_v7.4$ channels carrying mutations in the C-terminal region of S_4. (*A*) Representative ionic (*left*) and gating (*right*) current traces recorded from oocytes expressing wild-type, R6W, R6Q, and D1G channels, in response to the voltage protocols indicated. (*B* and *C*) *G/V* (*B*) and Q_{ON}/V (*C*) curves for the indicated channels. Continuous lines represent Boltzmann fits to the experimental data. (*D*) Time constants for Q_{ON} and ionic current activation at +40 mV ($n = 4$–9). (*E*) Time constants for Q_{OFF} and ionic current deactivation at −100 mV ($n = 4$–9).

were devoid of Cl^-, an experimental condition chosen to minimize the contribution of Ca^{2+}-dependent and Ca^{2+}-independent Cl^- currents abundantly expressed in the oocyte membrane, rules out a significant contribution of Cl^- ions.

Despite these technical limitations, the fact that the persistent noninactivating currents were larger than those recorded in oocytes expressing wild-type or any other mutant $K_v7.4$ channels, and that their magnitude was related to the number of functional channels, strongly suggests that they correspond to gating-pore currents similar to those generated upon the removal of specific basic residues in the VSD in several VGICs (37–42). The putative pore reported here opens on depolarization, indicating that the involved R4 residue occupies a deeper position in the resting state of the $K_v7.4$ VSD.

Finally, attempts to identify the depolarization-activated persistent currents caused by the R4Q mutation in the $K_v7.2$ channel background were not successful, likely because of the described low density of $K_v7.2$ channels in the oocyte membrane (data not shown).

Modeling and molecular dynamics of the $K_v7.4$ VSD

To follow up on the possibility of a gating pore, we generated a structural homology model for $K_v7.4$ using $K_v1.2$ as a template (43). Molecular dynamics (MD) simulations were performed on this homology model in an all-atom explicit-solvent environment to observe the region surrounding R4. In the activated configuration, the $K_v7.4$ VSD formed two hourglass-shaped water crevices separated by a plug (Fig. 5, *A* and *B*). A salt bridge between R4 and E136 in S_2 (Fig. 5, *A* and *B*) was also observed, which is responsible for the focused electric field in the membrane (37,44,45). Movie S1 shows that in $K_v7.4$ channels, the VSD is poorly permeant to water, allowing only very brief episodes of water flow during the entire 10-ns MD simulation. On the other hand, the R4Q mutation, by impeding the ionic interaction between R4 and E136, caused the upper and lower water crevices to nearly join as the plug dissolved (Fig. 5 *C*); MD experiments in $K_v7.4$ R4Q channels show a persistent water flux across the crevices throughout the 10-ns simulation (Movie S2).

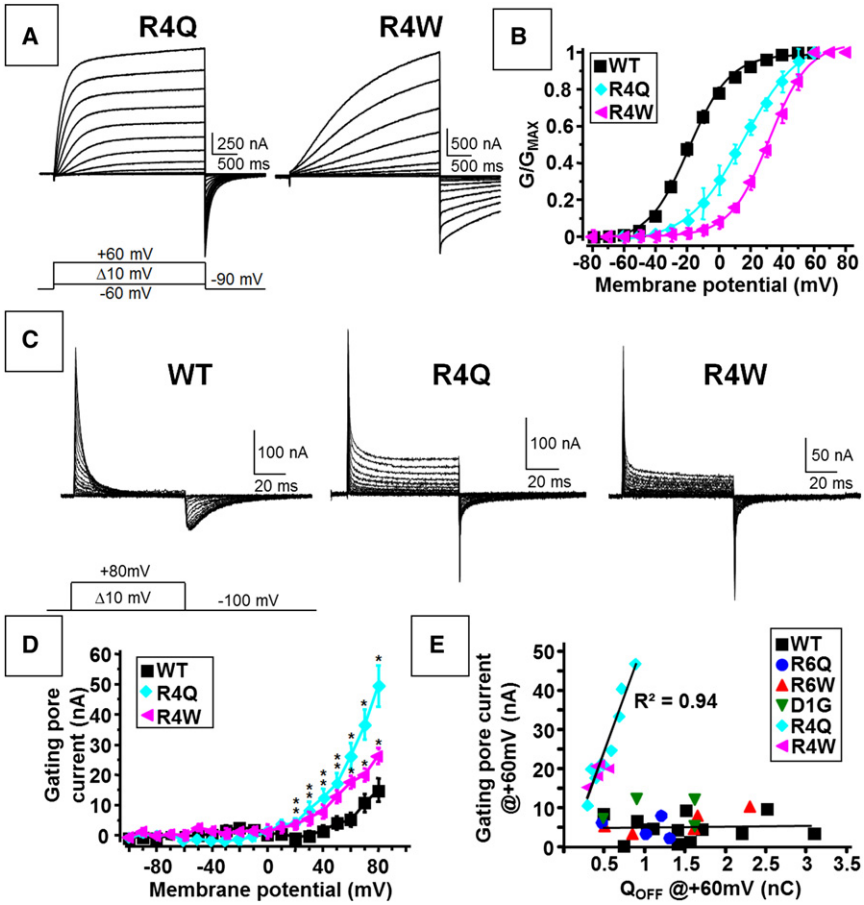

FIGURE 4 Ionic and gating currents from $K_v7.4$ channels carrying mutations in the central portion of S_4. (*A*) Representative macroscopic current traces elicited from oocytes expressing R4Q or R4W channels recorded in response to the indicated voltage protocol. (*B*) *G/V* curves for wild-type, R4Q, and R4W mutant channels. Continuous lines represent Boltzmann fits to the experimental data. (*C*) Representative gating current traces elicited from oocytes expressing wild-type, R4Q, or R4W channels, as indicated, recorded in response to the indicated voltage protocol. (*D*) Magnitude of the residual currents (gating-pore currents) calculated, after ionic current blockade, at the end of the voltage pulses from wild-type, R4Q, and R4W channels ($n = 5–10$). (*E*) Correlation between Q_{OFF} and gating-pore current magnitudes (both at + 60 mV) for the indicated channels. Each data point is from a single oocyte, from at least three separate batches. The two continuous lines represent linear regression fits for the data of wild-type and R4Q channels.

DISCUSSION

Mutation-induced changes in gating of VGICs often provide plausible pathogenetic explanations for channelopathies. In particular, changes in the sensitivity to voltage of homomeric $K_v7.2$ or heteromeric $K_v7.2/K_v7.3$ channels have been suggested to play a relevant role in the pathogenesis of BFNS as well as PNH (11–14). Gating-current analysis offers an in-depth view of channel gating properties, since it provides a direct assessment of VSD displacement during channel gating; however, to our knowledge, this technique has never been applied to the functional study of BFNS- or PNH-causing mutations. In this study, BFNS- and/or PNH-causing $K_v7.2$ mutations were investigated using $K_v7.4$ channels to correlate the mutation-induced changes in macroscopic current behavior with the altered function of the VSD, since gating currents from $K_v7.2$ channels could not be resolved.

When compared to $K_v7.2$, $K_v7.4$ channels show a high degree of sequence similarity in the VSD (~90%) and an identical distribution of charged residues within S_4; moreover, mutations in the VSD cause similar functional changes in gating in $K_v7.2$ or $K_v7.4$. In fact, charge neutralization of the R2 residue generated channels carrying voltage- and time-independent currents when incorporated in $K_v7.2$ (34) or $K_v7.4$ channels, as well as in $K_v7.1$ channels (35). This functional similarity revealed by the R2Q mutation appears unique among K_v7 channel members; indeed, in *Shaker* channels, the simultaneous neutralization of the R1, R2, and R3 charges is required to generate voltage-independent currents (46), a result suggestive of a lesser role of the R2 charge alone in resting-state VSD stabilization in *Shaker* channels; however, it should be remembered that the R3 residue in K_v7 channels is naturally neutralized by a Q residue.

Macroscopic currents from homomeric channels formed by all members of the K_v7 family are characterized by slow activation and deactivation kinetics, and by the absence of inactivation (22), except in the case of $K_v7.1$, which does exhibit inactivation (47). Gating current recordings from $K_v7.4$ channels revealed a poor coupling between charge movement and ionic currents, with Ig_{ON} decay being at least 10 times faster than ionic current activation. This indicates that the slow activation gating of $K_v7.4$ channels is not due to a slow movement of the VSD, and it suggests the existence of slower and less voltage-dependent transitions among closed states near the open state, a result also supported by the existence of a rising phase in Ig_{OFF} (28). Moreover, the fact that Ig_{OFF} kinetics closely match those of ionic current deactivation also suggests that the closure

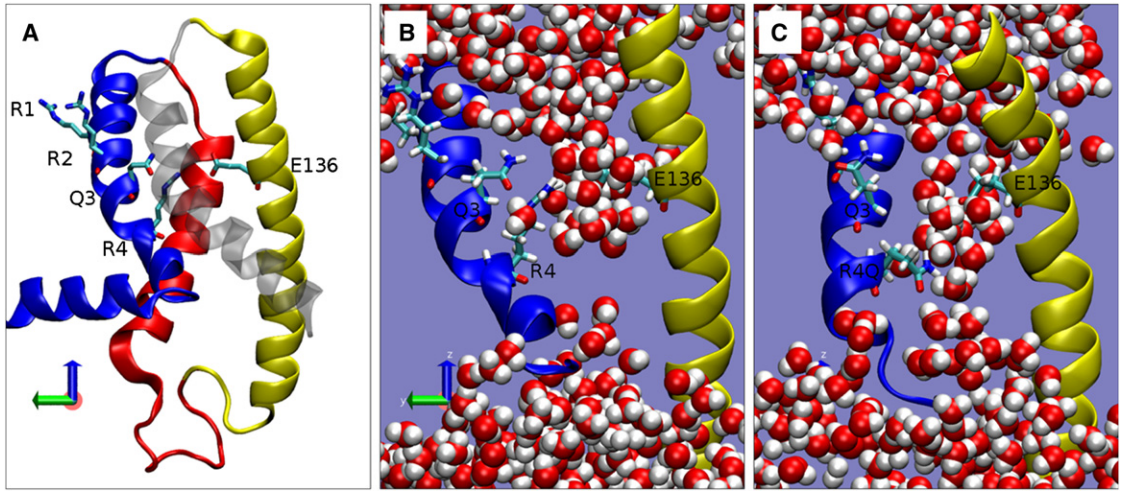

FIGURE 5 Molecular modeling of $K_v7.4$ and $K_v7.4$ R4Q VSDs. (*A*) Full $K_v7.4$ VSD in open/relaxed-state conformation after a 10-ns all-atom simulation, with components colored transparent gray (S1), yellow (S_2), red (S_3), and blue (S_4). (*B* and *C*) The salt-bridge interaction between R4 and E136 in S2 (*B*) is shown impeded by the R4Q mutation (*C*); also shown are the interactions involving the F143 residue in S_2. Both *B* and *C* show the VSD configurations at the end of molecular dynamics simulations (10 ns); the full movies of the 10-ns simulations for both wild-type and R4Q VSDs are provided as Movies S1 and S2, respectively.

of the pore may be rate-limiting for the VSD return to the resting state. In addition, poor coupling between VSD displacement (fast) and pore opening (slow) might also be responsible for the differences in macroscopic current kinetics observed between $K_v7.2$ and $K_v7.4$ homomeric channels (see Fig. 1); whether differences in S_4 uncharged residues, which are known to influence macroscopic gating in K_v7 cannels (13), contribute to this differential macroscopic current kinetics is yet to be explored (48).

In this work, we show that three mutations affecting charged residues located in the more distal portion of S_4 (R6Q, R6W, and D1G) similarly increased the rate of current activation and deactivation and decreased the sensitivity to voltage of the ionic current steady-state activation process by ~30 mV. Gating-current measurements from channels carrying these mutations revealed a slight (~10-mV) shift toward more depolarizing potentials and a decreased slope of the Q_{ON}/V curve; only minor effects were prompted by these mutations on Ig_{ON} decay kinetics, whereas Ig_{OFF} rose instantaneously and decayed faster. These results suggest that these mutations decrease the stability of the open state and of the active VSD configuration; however, the fact that they only caused a relatively mild rightward shift in the Q/V compared to the G/V curves suggests that the D1 and R6 residues do not directly participate in voltage sensing but rather may be involved in stabilizing the activated configuration of the VSD and allowing its slow electromechanical coupling with the pore opening process (27,43). Homology modeling of the $K_v7.4$ subunit to the open configuration of $K_v1.2$ revealed that R6 and D1 form ionized hydrogen bonds that stabilize the activated state of the VSD; in particular, R6 interacts with E146 in S_2, whereas D1 interacts with G222, W224, and K225 in the S_4-S_5 linker. Neutralization of R6 or D1 by BFNS-causing mutations would impede the formation of these hydrogen bonds, thereby leading to a marked destabilization of the active VSD configuration (Fig. S1 in the Supporting Material). In $K_v1.1$ channels, the R6Q mutation generated nonfunctional channels because of a maturation deficit; the R6K mutant, instead, like the R6 mutants herein described, accelerated Ig_{OFF} kinetics (49). In the same channels, mutations affecting residues located in the S_4 (50), the C-terminal region of the S_4-S_5 linker (51,52), the S_5 (53,54), and the S_6 (52,55) domains involved in stabilizing the activated state of the VSD all remove the Ig_{OFF} slow rising phase.

On the other hand, mutations affecting the R4 residue (R4Q and R4W), located more proximally along the S4 primary sequence and belonging to the first four voltage-sensing gating charges (1,2), dramatically decreased the ionic current activation and deactivation rates of $K_v7.4$ channels, with effects similar to those occurring in $K_v7.2$ (11,25,34). Upon pore current blockade, both R4Q and R4W channels generated very fast Ig_{ON}, followed by a small sustained current when depolarized. Upon membrane repolarization, Ig_{OFF} rose instantaneously and decayed rapidly; compared to wild-type channels, the Q_{OFF}/V curve for R4Q channels was right-shifted by +40 mV, also displaying a decreased slope. The sustained currents were specifically carried by R4Q or R4W channels, since they were never observed in oocytes expressing any other channel and, more important, their magnitude was directly proportional to the number of functional channels. Currents that have similar properties have been described in several VGICs upon the removal of specific basic residues in the VSD (37–42). These currents, defined as gating-pore currents or

ω currents, flow through water-filled regions of the protein (crevices or gating pores) created by specific conformations of the VSD and where the electric field is highly concentrated. In *Shaker* channels, although the substitution of R1 with a histidine residue generated a proton-selective pore that opened upon membrane hyperpolarization (37), the introduction at the corresponding position of smaller hydrophobic residues (A, C, S, or V) allowed permeation by alkali cations (Cs^+, Na^+, K^+, and guanidinum) (38). By contrast, depolarization-induced proton-selective currents were observed in R4H mutant *Shaker* channels (56). In our case, neutralization of R4 was associated with gating-pore currents activating at depolarized potentials, and it seems likely that the absence of the positive charge at R3, naturally replaced by a Q in all K_v7s, helps in the formation of the gating pore. It has been recently shown that neutralization of two sequential positively charged S4 Rs support gating-pore currents in *Shaker* channels (57). In a similar way, brain $Na_v1.2$ channels carried gating-pore currents upon membrane hyperpolarization when both R1 and R2 were neutralized, and upon membrane depolarization when R2 and R3 neutralizing mutations were introduced in domain II (39).

MD experiments confirmed the formation of a water pore in the active $K_v7.4$ R4Q VSD configuration, mainly as a consequence of the lack of an electrostatic interaction between R4 and the E136 residue in S2 (58); the resulting proximity of water molecules dramatically enhances ionic conduction across the crevices.

The results presented here, showing that gating-pore currents can be generated by mutations affecting R4 in the VSD of K_v7 channels, in addition to their structural implications, may be of crucial pathophysiological importance. Among over 80 $K_v7.2$ BFNS mutations, only two, both occurring at the R4 residue, have been described in families affected by skeletal muscle myokymia after BFNS (R4W (11)), or in the reported absence of BFNS (R4Q (25)); therefore, it seems likely that the specific functional consequences prompted by these mutations, which in addition to the gating-pore currents herewith described also include a positive shift in the voltage-dependent activation of the current and a dominant-negative effect exerted by mutant subunits on the wild-type channels (11,25), might contribute to the occurrence of myokymia. In fact, although K_v7 channels exert most of their physiological function around threshold values of membrane potentials, VSD displacement during prolonged depolarizations would trigger the formation of a gating pore and allow inward currents carried mainly by Na^+ ions. Such inward Na^+ currents would provide a persistent depolarizing force that would contribute to the axonal hyperexcitability characterizing the myokymic phenotype. Similar effects would also be triggered if protons, rather than Na^+ ions, significantly permeated the gating pore (59). $K_v7.2$ channels are expressed at nodes of Ranvier in peripheral myelinated fibers, particularly in large motor axons, and their activation reduces intrinsic excitability (60). Gating-pore currents in S_4 mutants of $Na_v1.4$ channels contribute to hypokalemic (40,61) or normokalemic (41) periodic paralysis in skeletal muscle (42). Moreover, persistent inward Na^+ currents have been identified in $Na_v1.1$ channels carrying gain-of-function mutations responsible for generalized epilepsy with febrile seizure plus, another epileptic channelopathy (62).

In conclusion, the results presented here reveal what we believe are novel insights into the molecular mechanism of voltage sensing in K_v7 channels, provide plausible and previously unexplored biophysical mechanisms to account for the pathogeneses of hyperexcitability diseases caused by mutations in the VSD of these channels, and might be of relevance for the development of drugs targeting K_v7 VSD and acting as gating modifiers (36). With this in mind, gating-pore blockers have been recently proposed as therapeutically useful in preventing or relieving attacks of weakness in patients with hypokalemic periodic paralysis caused by mutations in the VSD of the skeletal muscle $Na_v1.4$ channels (63).

SUPPORTING MATERIAL

A figure and two movies are available at http://www.biophysj.org/biophysj/supplemental/S0006-3495(12)00204-4.

We are deeply indebted to Prof. Thomas J. Jentsch (Department of Physiology and Pathology of Ion Transport, Leibniz-Institut für Molekulare Pharmakologie, Berlin-Buch, Germany), for pTLN-K_v7 plasmids, Ludivine Frezza and Elisabetta Panza for initial help with molecular biology, and Carlos A. Villalba-Galea for initial help with the electrophysiology experiments.

This study was supported by grants from Telethon (GP07125), E-Rare (JTC 2007), the Fondazione San Paolo - IMI (Project Neuroscience), and PRIN 2009 to M.T., and from the National Institutes of Health (GM030376) to F.B.

REFERENCES

1. Aggarwal, S. K., and R. MacKinnon. 1996. Contribution of the S4 segment to gating charge in the *Shaker* K^+ channel. *Neuron.* 16:1169–1177.
2. Seoh, S. A., D. Sigg, …, F. Bezanilla. 1996. Voltage-sensing residues in the S2 and S4 segments of the *Shaker* K^+ channel. *Neuron.* 16:1159–1167.
3. Larsson, H. P., O. S. Baker, …, E. Y. Isacoff. 1996. Transmembrane movement of the shaker K^+ channel S4. *Neuron.* 16:387–397.
4. Yusaf, S. P., D. Wray, and A. Sivaprasadarao. 1996. Measurement of the movement of the S4 segment during the activation of a voltage-gated potassium channel. *Pflugers Arch.* 433:91–97.
5. Yang, N., A. L. George, Jr., and R. Horn. 1996. Molecular basis of charge movement in voltage-gated sodium channels. *Neuron.* 16:113–122.
6. Catterall, W. A. 2010. Ion channel voltage sensors: structure, function, and pathophysiology. *Neuron.* 67:915–928.
7. Campos, F. V., B. Chanda, …, F. Bezanilla. 2007. Two atomic constraints unambiguously position the S4 segment relative to S1

and S2 segments in the closed state of *Shaker* K channel. *Proc. Natl. Acad. Sci. USA.* 104:7904–7909.

8. Tao, X., A. Lee, …, R. MacKinnon. 2010. A gating charge transfer center in voltage sensors. *Science.* 328:67–73.
9. Chen, X., Q. Wang, …, J. Ma. 2010. Structure of the full-length *Shaker* potassium channel $K_v1.2$ by normal-mode-based x-ray crystallographic refinement. *Proc. Natl. Acad. Sci. USA.* 104:11352–11357.
10. Lacroix, J. J., and F. Bezanilla. 2011. Control of a final gating charge transition by a hydrophobic residue in the S2 segment of a K^+ channel voltage sensor. *Proc. Natl. Acad. Sci. USA.* 108:6444–6449.
11. Dedek, K., B. Kunath, …, O. K. Steinlein. 2001. Myokymia and neonatal epilepsy caused by a mutation in the voltage sensor of the KCNQ2 K^+ channel. *Proc. Natl. Acad. Sci. USA.* 98:12272–12277.
12. Castaldo, P., E. M. del Giudice, …, M. Taglialatela. 2002. Benign familial neonatal convulsions caused by altered gating of KCNQ2/KCNQ3 potassium channels. *J. Neurosci.* 22:RC199.
13. Soldovieri, M. V., M. R. Cilio, …, M. Taglialatela. 2007. Atypical gating of M-type potassium channels conferred by mutations in uncharged residues in the S4 region of KCNQ2 causing benign familial neonatal convulsions. *J. Neurosci.* 27:4919–4928.
14. Miceli, F., M. V. Soldovieri, …, M. Taglialatela. 2011. The voltage-sensing domain of $K_v7.2$ channels as a molecular target for epilepsy-causing mutations and anticonvulsants. *Front Pharmacol.* 2:2.
15. Biervert, C., B. C. Schroeder, …, O. K. Steinlein. 1998. A potassium channel mutation in neonatal human epilepsy. *Science.* 279:403–406.
16. Singh, N. A., C. Charlier, …, M. Leppert. 1998. A novel potassium channel gene, KCNQ2, is mutated in an inherited epilepsy of newborns. *Nat. Genet.* 18:25–29.
17. Charlier, C., N. A. Singh, …, M. Leppert. 1998. A pore mutation in a novel KQT-like potassium channel gene in an idiopathic epilepsy family. *Nat. Genet.* 18:53–55.
18. Cooper, E. C., E. Harrington, …, L. Y. Jan. 2001. M channel KCNQ2 subunits are localized to key sites for control of neuronal network oscillations and synchronization in mouse brain. *J. Neurosci.* 21:9529–9540.
19. Pan, Z., T. Kao, …, E. C. Cooper. 2006. A common ankyrin-G-based mechanism retains KCNQ and NaV channels at electrically active domains of the axon. *J. Neurosci.* 26:2599–2613.
20. Devaux, J. J., K. A. Kleopa, …, S. S. Scherer. 2004. KCNQ2 is a nodal K^+ channel. *J. Neurosci.* 24:1236–1244.
21. Martire, M., P. Castaldo, …, M. Taglialatela. 2004. M channels containing KCNQ2 subunits modulate norepinephrine, aspartate, and GABA release from hippocampal nerve terminals. *J. Neurosci.* 24:592–597.
22. Soldovieri, M. V., F. Miceli, and M. Taglialatela. 2011. Driving with no brakes: molecular pathophysiology of K_v7 potassium channels. *Physiology (Bethesda).* 26:365–376.
23. Soldovieri, M. V., P. Castaldo, …, M. Taglialatela. 2006. Decreased subunit stability as a novel mechanism for potassium current impairment by a KCNQ2 C terminus mutation causing benign familial neonatal convulsions. *J. Biol. Chem.* 281:418–428.
24. Chung, H. J., Y. N. Jan, and L. Y. Jan. 2006. Polarized axonal surface expression of neuronal KCNQ channels is mediated by multiple signals in the KCNQ2 and KCNQ3 C-terminal domains. *Proc. Natl. Acad. Sci. USA.* 103:8870–8875.
25. Wuttke, T. V., K. Jurkat-Rott, …, H. Lerche. 2007. Peripheral nerve hyperexcitability due to dominant-negative KCNQ2 mutations. *Neurology.* 69:2045–2053.
26. Sadewa, A. H., T. H. Sasongko, …, H. Nishio, Gunadi. 2008. Germline mutation of KCNQ2, p.R213W, in a Japanese family with benign familial neonatal convulsion. *Pediatr. Int.* 50:167–171.
27. Miceli, F., M. V. Soldovieri, …, M. Taglialatela. 2009a. Neutralization of a unique, negatively-charged residue in the voltage sensor of $K_v7.2$ subunits in a sporadic case of benign familial neonatal seizures. *Neurobiol. Dis.* 34:501–510.
28. Miceli, F., M. R. Cilio, …, F. Bezanilla. 2009b. Gating currents from neuronal $K_v7.4$ channels: general features and correlation with the ionic conductance. *Channels (Austin).* 3:274–283.
29. Taglialatela, M., L. Toro, and E. Stefani. 1992. Novel voltage clamp to record small, fast currents from ion channels expressed in *Xenopus* oocytes. *Biophys. J.* 61:78–82.
30. Stefani, E., and F. Bezanilla. 1998. Cut-open oocyte voltage-clamp technique. *Methods Enzymol.* 293:300–318.
31. Zaika, O., C. C. Hernandez, …, M. S. Shapiro. 2008. Determinants within the turret and pore-loop domains of KCNQ3 K^+ channels governing functional activity. *Biophys. J.* 95:5121–5137.
32. Li, Y., N. Gamper, and M. S. Shapiro. 2004. Single-channel analysis of KCNQ K^+ channels reveals the mechanism of augmentation by a cysteine-modifying reagent. *J. Neurosci.* 24:5079–5090.
33. Etxeberria, A., I. Santana-Castro, …, A. Villarroel. 2004. Three mechanisms underlie KCNQ2/3 heteromeric potassium M-channel potentiation. *J. Neurosci.* 24:9146–9152.
34. Miceli, F., M. V. Soldovieri, …, M. Taglialatela. 2008. Gating consequences of charge neutralization of arginine residues in the S4 segment of $K_v7.2$, an epilepsy-linked K^+ channel subunit. *Biophys. J.* 95:2254–2264.
35. Panaghie, G., and G. W. Abbott. 2007. The role of S4 charges in voltage-dependent and voltage-independent KCNQ1 potassium channel complexes. *J. Gen. Physiol.* 129:121–133.
36. Peretz, A., L. Pell, …, B. Attali. 2010. Targeting the voltage sensor of $K_v7.2$ voltage-gated K^+ channels with a new gating-modifier. *Proc. Natl. Acad. Sci. USA.* 107:15637–15642.
37. Starace, D. M., and F. Bezanilla. 2004. A proton pore in a potassium channel voltage sensor reveals a focused electric field. *Nature.* 427:548–553.
38. Tombola, F., M. M. Pathak, and E. Y. Isacoff. 2005. Voltage-sensing arginines in a potassium channel permeate and occlude cation-selective pores. *Neuron.* 45:379–388.
39. Sokolov, S., T. Scheuer, and W. A. Catterall. 2005. Ion permeation through a voltage-sensitive gating pore in brain sodium channels having voltage sensor mutations. *Neuron.* 47:183–189.
40. Sokolov, S., T. Scheuer, and W. A. Catterall. 2007. Gating pore current in an inherited ion channelopathy. *Nature.* 446:76–78.
41. Sokolov, S., T. Scheuer, and W. A. Catterall. 2008. Depolarization-activated gating pore current conducted by mutant sodium channels in potassium-sensitive normokalemic periodic paralysis. *Proc. Natl. Acad. Sci. USA.* 105:19980–19985.
42. Cannon, S. C. 2010. Voltage-sensor mutations in channelopathies of skeletal muscle. *J. Physiol.* 588:1887–1895.
43. Long, S. B., E. B. Campbell, and R. Mackinnon. 2005. Voltage sensor of $K_v1.2$: structural basis of electromechanical coupling. *Science.* 309:903–908.
44. Ahern, C. A., and R. Horn. 2005. Focused electric field across the voltage sensor of potassium channels. *Neuron.* 48:25–29.
45. Jogini, V., and B. Roux. 2007. Dynamics of the $K_v1.2$ voltage-gated K^+ channel in a membrane environment. *Biophys. J.* 93:3070–3082.
46. Bao, H., A. Hakeem, …, M. D. Rayner. 1999. Voltage-insensitive gating after charge-neutralizing mutations in the S4 segment of *Shaker* channels. *J. Gen. Physiol.* 113:139–151.
47. Pusch, M., R. Magrassi, …, F. Conti. 1998. Activation and inactivation of homomeric KvLQT1 potassium channels. *Biophys. J.* 75:785–792.
48. Smith-Maxwell, C. J., J. L. Ledwell, and R. W. Aldrich. 1998. Uncharged S4 residues and cooperativity in voltage-dependent potassium channel activation. *J. Gen. Physiol.* 111:421–439.
49. Perozo, E., L. Santacruz-Toloza, …, D. M. Papazian. 1994. S4 mutations alter gating currents of *Shaker* K channels. *Biophys. J.* 66: 345–354.
50. Ledwell, J. L., and R. W. Aldrich. 1999. Mutations in the S4 region isolate the final voltage-dependent cooperative step in potassium channel activation. *J. Gen. Physiol.* 113:389–414.

51. Schoppa, N. E., and F. J. Sigworth. 1998. Activation of *Shaker* potassium channels. III. An activation gating model for wild-type and V2 mutant channels. *J. Gen. Physiol.* 111:313–342.

52. Batulan, Z., G. A. Haddad, and R. Blunck. 2010. An intersubunit interaction between S4-S5 linker and S6 is responsible for the slow off-gating component in *Shaker* K^+ channels. *J. Biol. Chem.* 285: 14005–14019.

53. Kanevsky, M., and R. W. Aldrich. 1999. Determinants of voltage-dependent gating and open-state stability in the S5 segment of *Shaker* potassium channels. *J. Gen. Physiol.* 114:215–242.

54. Soler-Llavina, G. J., T. H. Chang, and K. J. Swartz. 2006. Functional interactions at the interface between voltage-sensing and pore domains in the *Shaker* K_v channel. *Neuron.* 52:623–634.

55. Hackos, D. H., T. H. Chang, and K. J. Swartz. 2002. Scanning the intracellular S6 activation gate in the shaker K^+ channel. *J. Gen. Physiol.* 119:521–532.

56. Starace, D. M., and F. Bezanilla. 2001. Histidine scanning mutagenesis of basic residues of the S4 segment of the shaker k^+ channel. *J. Gen. Physiol.* 117:469–490.

57. Gamal El-Din, T. M., H. Heldstab, …, N. G. Greeff. 2010. Double gaps along *Shaker* S4 demonstrate omega currents at three different closed states. *Channels (Austin).* 4:93–100.

58. Papazian, D. M., X. M. Shao, …, D. H. Wainstock. 1995. Electrostatic interactions of S4 voltage sensor in *Shaker* K^+ channel. *Neuron.* 14:1293–1301.

59. Matthews, E., and M. G. Hanna. 2010. Muscle channelopathies: does the predicted channel gating pore offer new treatment insights for hypokalaemic periodic paralysis? *J. Physiol.* 588:1879–1886.

60. Schwarz, J. R., G. Glassmeier, …, H. Bostock. 2006. KCNQ channels mediate IKs, a slow K^+ current regulating excitability in the rat node of Ranvier. *J. Physiol.* 573:17–34.

61. Struyk, A. F., and S. C. Cannon. 2007. A Na^+ channel mutation linked to hypokalemic periodic paralysis exposes a proton-selective gating pore. *J. Gen. Physiol.* 130:11–20.

62. Lossin, C., D. W. Wang, …, A. L. George, Jr. 2002. Molecular basis of an inherited epilepsy. *Neuron.* 34:877–884.

63. Sokolov, S., T. Scheuer, and W. A. Catterall. 2010. Ion permeation and block of the gating pore in the voltage sensor of $Na_V1.4$ channels with hypokalemic periodic paralysis mutations. *J. Gen. Physiol.* 136: 225–236.